Am J Physiol Endocrinol Metab 331: E184–E197, 2026.
First published June 30, 2026; doi:10.1152/ajpendo.00061.2026

american physiological society

AMERICAN JOURNAL OF PHYSIOLOGY
ENDOCRINOLOGY AND METABOLISM

RESEARCH ARTICLE

Women's Health Research and Pregnancy, Postnatal Conditions, Endometriosis, Polycystic Ovarian Syndrome, Preeclampsia

Chemogenetic placental activation and proteomic extracellular vesicle signatures predict functional roles across pregnancy and postpartum

Geoffrey A. Dunn, Arthur S. Feltrin, Rodrigo Orso, and Tracy L. Bale

Division of Neuroscience, Department of Psychiatry, School of Medicine, University of Colorado Anschutz Medical Campus, Aurora, Colorado, United States

Abstract

Mechanisms underlying homeostatic regulation of maternal health during pregnancy and the postpartum period are critical yet remain understudied. Extracellular vesicles (EVs) are vital sources of cell-to-cell communication that maintain homeostasis and are at their highest circulating concentration during pregnancy. Recent studies have implicated EVs and their cargo as facilitators in important physiological functions during pregnancy, including glucose and immune regulation, but precise mechanisms are not known. In this study, we aimed to compare changes in EVs and their protein cargo using unbiased proteomic analyses across pregnancy and postpartum periods to assert unique EV functions. As expected, we found significantly higher EV concentrations during pregnancy relative to nonpregnant and postpartum groups. We identified unique EV protein profiles across groups, suggesting EVs were highly responsive to their current environment and performing unique functions. Surprisingly, while postpartum mice had similar EV concentrations as nonpregnant mice, their EVs had the least overlap in protein composition between groups and the greatest number of proteins clustered in a biological function—a significant reduction around cell adhesion processes postpartum. Lastly, to examine a homeostatic role for maternal circulating EVs, we used a novel chemogenetic approach to control dynamic EV secretion and measured changes in maternal glucose regulation. We found that an acute increase in circulating EVs reduced maternal glucose sensitivity, keeping glucose levels elevated longer following a glucose challenge. In summary, these results demonstrate the unique EV protein cargo changes that occur in pregnancy and postpartum and their potential importance in maintenance of maternal health.

NEW & NOTEWORTHY Extracellular vesicles in maternal circulation express unique proteomic cargo profiles across pregnancy and postpartum. Chemogenetic activation of the placental secretory pathway releases extracellular vesicles into maternal circulation that influence maternal glucose regulation.

chemogenetic; extracellular vesicles; postpartum; pregnancy; proteomics

INTRODUCTION

Biological factors influencing maternal health during pregnancy and the postpartum period are understudied, even as rates of maternal morbidity and mortality remain high (1). Pregnancy and postpartum are biologically unique periods in the lifespan, with dynamic and significant changes occurring in maternal physiology and a high demand for mechanisms important to systemic homeostasis, especially those involved in glucose and immune regulation. Adverse health during pregnancy, including preterm birth, gestational diabetes, and preeclampsia, is strong predictor of poor postpartum health that may last for years or decades after birth (2–5). Although early identification of elevated risk can ameliorate or prevent maternal pathophysiology, we still lack a sufficient understanding of underlying mechanisms or validated biomarkers that significantly contribute to improving maternal health.

Extracellular vesicles (EVs) are of increasing focus across a number of disease areas for their key role in systemic communication and coordination, especially with the immune system, and have been identified as having high potential to serve as predictive biomarkers (6–12). EVs are biological nanoparticles secreted by all tissues tasked with transporting biological cargo, including small RNAs, proteins, and lipids, throughout the body, and are a heterogeneous population comprised of several subtypes, including smaller-sized exosomes and larger-sized microvesicles. In pregnancy, EVs are one of the most dynamic

Correspondence: T. L. Bale (tracy.bale@cuanschutz.edu).
Submitted 11 February 2026 / Revised 18 May 2026 / Accepted 11 June 2026

and abundant biological signals in circulation. Maternal levels increase 3–4-fold, in part due to EV secretion from the placenta (8, 13, 14). The increased EV concentration during pregnancy supports proposed critical roles for these nanoparticles in diverse functions including embryo implantation, immune regulation, angiogenesis, glucose regulation, and the onset of parturition (7, 15–18). Although much of this work in this area has contributed to our understanding of roles for EVs important to maternal health, the precise mechanisms for temporal changes in EV biogenesis and composition remain less clear, in part due to insufficient tools with which we can ask such questions (11). The functional dynamics of placental-derived EVs is of particular interest because it could identify key processes for sensing and regulating the maternal environment, a valuable step toward biomarker confirmation and potential novel therapeutic targets. Importantly, although not yet examined, removal of the placenta at birth likely results in a rapid reduction in EV concentration in maternal circulation. Thus, EV signaling during the transition from pregnancy to the postpartum period may play a similar role in regulating the maternal environment after birth.

Previous studies by our group and others using in vivo and in vitro models identified an important role for circulating EVs in maternal glucose homeostasis. In mice, we previously isolated EVs from pregnant females and injected them into nonpregnant mice, producing a significant change in glucose dynamics (19). However, a limitation of this method is an inability to temporally increase circulating levels of EVs in the pregnancy environment due to an already profoundly high EV concentration. In the current studies, we first examined temporal changes in key EV characteristics and, using an unbiased approach, also assessed changes in EV protein cargo between nonpregnant, pregnant, and postpartum mice, focusing on the functional interpretation of protein pathways and tissues involved to define what EVs are likely doing at that time point. We hypothesized EVs would increase in concentration during pregnancy and decrease in postpartum to similar levels as nonpregnant mice. Furthermore, we hypothesized EVs would exhibit unique proteomic signatures at each time point reflecting dynamic changes in signaling required for maintaining homeostasis. Next, to specifically probe circulating EV contribution to maternal homeostasis, we "highjacked" the trophoblast cell secretory pathway using a chemogenetic approach to drive dynamic EV secretion. Extracellular vesicles are released through diverse intracellular signals, with calcium-based signal transduction via GPCRs constituting a common signaling pathway (20). Using a transgenic mouse model to express the metabotropic DREADD receptor specifically in placental cells of trophoblast origin, we activated the secretory pathway of trophoblast cells to elicit an increase in extracellular vesicles in maternal circulation. Measuring changes in glucose homeostasis as a proxy for control of maternal physiology, we investigated the effect of this acute increase in EV concentration in vivo and in real-time in the pregnancy state. We hypothesized chemogenetic increases in EVs secreted from the placenta would impact maternal glucose regulation.

METHODS

Animals

Mice used in these studies were bred in-house and were derived from a mixed-background (C57Bl/6:129) strain. Virgin dams were between 10–16 wk old, and only litters of 4–12 pups were included in analyses. To establish pregnancy, dams were paired with sires 1700–0800. Copulation plugs were checked 0800, and embryonic day 0.5 (E0.5) was considered 1200 on the day a plug was identified. Dams were evaluated on E12.5 and postpartum day 2. E12.5 is the earliest time point when the mouse placenta is fully differentiated and exerts a significant influence on maternal circulating EVs (21). All experiments/collections were conducted between 1400 and 1700.

Mice used to examine the specific signaling of EVs from the placenta during pregnancy using chemogenetic methods were double-heterozygous CYP19-Cre (P.Cre+/−) (22); hM3Dq Designer Receptors Exclusively Activated by Designer Drugs (Gq-DREADD) mice (DRD+/−; Jax stock #026220) to specifically target trophoblast-derived cells in the placenta following Clozapine-N-oxide (CNO) drug administration. Dams were evaluated on E15.5, and all experiments/collections were conducted between 1400and 1700. All dams, P.Cre+/Gq-DREADD+ (DRD+, $n = 5$) and wild type (WT, $n = 4$), received an intraperitoneal injection (ip) of CNO (1 mg/kg). After 5 min, mice were anesthetized, blood was collected via cardiac puncture, and EVs were isolated as described in *EV Isolation*. Fetal tail DNA was isolated from each offspring and used for genotyping and sex determination.

All animals used in this study were euthanized using a precision vaporizer with an induction chamber and waste gas scavenger, in which isoflurane was administered in 2.5% O2 for 1 min. Decapitation was performed after cardiac puncture to ensure euthanasia. Mice were administered chow (Teklad 2920X global soy protein-free extruded; Madison, WI) and water ad libitum. Lights were maintained on a 10:14 schedule with lights on at 0600 h and lights off at 2000 h. All procedures in this study were approved by the University of Colorado Anschutz Medical Campus Institutional Animal Care and Use Committee. All procedures were conducted in accordance with the National Institutes of Health Guide for the Care and Use of Laboratory Animals.

Glucose Tolerance Test

Glucose tolerance test (GTT) was performed as previously reported (19). Briefly, E15.5 pregnant dams, DRD+ ($n = 7$) or WT ($n = 8$), were fasted for 6 h beginning at 0800. Dams received a 1 mg/kg CNO ip followed by a second ip of glucose (3 mg/g). Glucose readings were collected at 0, 10, 20, 30, 60, 90, and 120 min using the Contour Nex Blood Glucose Monitoring System (Bayer Co, Germany). Following the GTT, dams were euthanized and fetal tails collected to evaluate litter P.Cre and DRD genotyping.

EV Isolation

Roughly 1 mL of blood was collected via cardiac puncture using 23 G syringes (Becton Dickinson). Blood was placed into 1.5-mL DNA LoBind Tubes (Eppendorf) with 50 μL of 50 mM EDTA (Sigma) and placed on ice. Blood was

immediately centrifuged at 2,000 rcf for 12 min at 4°C. Plasma was then aliquoted and stored at −80°C until further EV isolation steps. EVs were isolated from 350 μL of plasma. Plasma was mixed with 250 μL of freshly filtered (0.22-μm pore size filter, Sigma) phosphate-buffered saline (PBS). This mixture was centrifuged at 2,000 rcf for 30 min at 4°C to clear large cellular debris. Roughly 550 μL of supernatant was transferred and centrifuged again at 12,000 rcf for 45 min at 4°C for further purification and pellet cell debris. EVs were then immediately isolated from the resultant supernatant via size-exclusive chromatography using IZON qEVoriginal Gen 2 70-nm columns in the IZON Automate Fraction Collector (Izon Science). Fractions 1–3 were combined and stored at −80°C until analysis could be performed, at which time samples were thawed on ice.

EV Nanoparticle Tracking Analysis

The concentration, size and zeta-potential of isolated EVs were measured with a ZetaView MONO Nanoparticle Tracking Analysis Microscope (Particle Metrix) as described previously (19). Briefly, thawed isolated EV samples were diluted in freshly filtered (0.22-μm pore size filter, Sigma) Milli-Q water to a final concentration in the range of 10^7 particles/mL (∼200 particles per frame).

EV Transmission Electron Microscopy

A 10-μL drop of sample was applied to a freshly glow-discharged 300 mesh formvar and carbon-coated grid (Electron Microscopy Sciences) for 5 min and blotted with filter paper. The grid was then washed by applying 10-μL water on the grid and blotted with a Whatman filter paper. Finally, the grids were stained with 10 μL of 2% uranyl acetate solution. After blotting, the grids were allowed to dry. Samples were imaged on a JEM-120i (JEOL) at 120 kV with a low-mount 15-megapixel NanoSprint15LMarkII camera (AMT Imaging).

EV Protein Extraction and Western Immunoblotting

Biochemical analysis by Western blotting was used to identify EV-specific proteins as described previously (23). Briefly, EVs were lysed in radioimmunoprecipitation assay (RIPA) buffer (EMD Milllipore, 20–188) with 0.1% SDS and cOmplete EDTA-free protease inhibitor (Roche Diagnostics, 11836170001). Samples were shaken for 15 min at 3,000 RPM at 4°C using a Disruptor Genie (Scientific Industries) and stored at −80°C. Gel electrophoresis was performed using NuPAGE 4–12% Bis-Tris gel (Invitrogen, 0321) loaded with 12 μg of protein for cell extract samples or protein extracted from EV samples. After transfer of proteins to a nitrocellulose membrane (Life Technologies, LC2000), membranes were blocked with Intercept blocking buffer-PBS (LI-COR, 927–70001) with 0.1% Tween-20.

Membranes were immunoblotted with primary antibodies for EV-specific proteins: rabbit anti-Annexin A2 (1:500; Abcam, AB178677) and rabbit anti-CD9 (1:500; Invitrogen, MA5-31980), followed by incubation in IRDye 800CW-conjugated donkey anti-rabbit secondary (1:5,000; LI-COR, 925-32213).

EV Proteomics

Dried purified EV samples were lysed, reduced, alkylated, digested with a trypsin/Lys-C mixture, and resultant peptides cleaned up using the Preomics iST 96x HT Kit by following the protocol for pelleted cells and precipitate proteins provided with the kit, similar to a previous publication (24). Briefly, samples were lysed in 50 μL of lysis buffer by vortexing for 2 min and then bath sonicated for 5 min before being heated at 90°C for 10 min. Trypsin/LysC (50 μL) mixture was then added, and samples were digested for 2 h at 37°C. The protocol was then followed exactly as stated. Briefly, enzyme reactivity was quenched with the stop buffer, and resultant peptide mixtures were transferred to SPE cartridges and cleaned up using the two wash buffers, and peptides were eluted into the MTP plate using the elution buffer. Samples were then transferred to individual 1.5-mL microfuge tubes and dried down by SpeedVac at 45°C for ∼90 min before freezing at −80°C. Samples were resuspended in 16 μL of LC-LOAD buffer provided with the Preomics kit by bath sonicating for 2 min followed by vortexing for 30 min. Peptide amounts were then quantified by BCA assay using the Pierce BCA Protein BCA Assay Kit and a NanoDrop Microvolume Spectrophotometer. Following quantitation, all samples were equalized to 0.164 μg/μL using additional LC-LOAD buffer. An aliquot of each sample was taken to make a pooled quality control sample that was injected every 12 samples to track instrument variance across the run.

Sample (4 μL) was loaded on an OrbiTrap Eclipse Mass Spectrometer (Thermo Fisher Scientific) for liquid chromatography-tandem mass spectrometry (LC-MS/MS) analysis similar to a previous publication (25). Samples were loaded onto an Acclaim Pepmap 100 C18 75 μm × 2 cm trapping column and chromatographically resolved online using an EASY-Spray Pepmap RSLC C18 75 μm × 25 cm 2-μm analytical column (Thermo Scientific) using an Ultimate 3000 RSLCnano LC system at 40°C. Mobile phases consisted of water + 0.1% formic acid (A) and 100% acetonitrile + 0.1% formic acid (B). Samples were loaded onto the enrichment column at an isocratic flow of 5 μL/min of 2% vol/vol ACN containing 0.1% vol/vol formic acid for 5 min before the enrichment column was switched in-line with the analytical column. Samples were chromatographically separated at a flow rate of 300 nL/min using a gradient of *i*) 0–4.5 min at 3% B; *ii*) 4.5–7 min, 3–7% B; *iii*) 7–54 min, 7.0–24.5% B; *iv*) 54–59 min, 24.5–33% B; *v*) 59–61 min, 33% to 80% B; *vi*) 61–66 min, 80% B; *vii*) 66–67 min, 80% to 3% and equilibrated at 3% B for 12 min before the next sample injection. For data-independent acquisition (DIA) experiments, MS1 scans were performed in the Orbitrap Detector at 120,000 resolution from 350 to 1,400 m/z in profile mode. Full MS automatic gain control (AGC) target was 250% with a maximum injection time (IT) of 50 ms. AGC target value for fragment spectra was set at 1000%; 50 windows of 13.7 Da were used with an overlap of 1 Da from 361–1,046 m/z in the precursor range. Resolution was set to 15,000 and maximum IT to 22 ms. Fragmentation was performed using HCD at a normalized collision energy of 30% from 200–2,000 m/z. All data were acquired in centroid mode using positive polarity.

DIA-MS data were searched and quantified in DIANN 2.2.0 using a spectral library-free search against the one protein sequence per gene *Mus musculus* reference proteome (Proteome ID UP000000589) in the UniProt Database (26). The predicted library was generated using Trypsin/P with two missed cleavages and fixed carbamidomethylation (C) and variable oxidation (M) modifications, with the

maximum variable modification set to 3. The peptide length range was set to 6–30 amino acids, precursor charge 1–4, precursor m/z 300–1,800, and fragment ion m/z range 200–2,000. Data was searched using a mass accuracy of 12 ppm (MS2), MS1 accuracy of 2.5 ppm, scan window of 8, Generate spectral library selected, precursor FDR (%) of 1.0, match between runs and protein inference were enabled with Generic scoring and NNs (cross-validated) machine learning. The quantification strategy used was Quant UMS (high accuracy) with RT-dependent cross-run normalization (27).

Statistics

Sample size, mean, and standard error of the mean (SE) are reported in the text and figure legends. GraphPad prism (v. 10.6.1) was used for visualization and statistics where appropriate. For experiments comparing two groups, unpaired *t* tests were used. Where experiments included three or more groups, one-way analysis of variance (ANOVA) testing with Tukey post hoc tests was used, with significance determined at an α level of 0.05. Analysis of glucose metabolic testing used repeated-measure ANOVAs with Tukey post hoc tests. All statistical comparisons and outputs are detailed in Supplemental Table S1. GraphPad Prism and BioRender were used to generate figures.

For analysis of proteomic data, we used open-access software MetaboAnalyst 6.0 (28). To accommodate skewed data and large amounts of missing values, input proteomic data underwent left-censored data estimation, which imputes missing values with 1/5 of the minimum positive value. Next, protein concentrations were normalized by sum, followed by a log2 transformation. Finally, values were scaled using a mean-centered and divided by the standard deviation of each variable method. Processed concentrations of detected proteins were analyzed using PCA plots, and significant differences in distributions were tested through permutational analysis of variance (PERMANOVA) using Euclidean distance, with significance determined at an α level of 0.05 (29). Detection of significant differentially expressed individual proteins used *t* tests using the Benjamini–Hochberg procedure with FDR Q-value = 0.05 to correct for multiple comparisons and $|\log2FC| \geq 0.2$. Functional proteomic enrichment analysis and visualization was performed using the STRING database (v. 12.0) utilizing GO terminology databases including Biological Process, Molecular Function, and Cellular Component at an FDR threshold of ≤ 0.05 (30). Protein-protein interaction (PPI) networks were created using the full STRING network, with a required score of 0.400 and an FDR stringency of 0.05. After network creation, all active interaction sources were used to visualize network edges. Cluster analysis used a k-means cluster algorithm with three defined clusters to group proteins often coexpressed in functional signaling or biological processes.

RESULTS

EVs Rise during Pregnancy and Fall in Early Postpartum but Reflect Unique Proteomic Signatures at Each Time Point

To test how characteristics and protein cargo of EVs in circulation change across pregnancy and postpartum, we collected plasma samples from age-matched nonpregnant females, E12.5 dams, and postpartum day 2 (PPD2). We observed higher circulating EV concentrations during pregnancy compared with both nonpregnant mice and PPD2 dams (Fig. 1, *A* and *B*, one-way ANOVA, $F_{2,\ 13} = 6.752$, $P < 0.01$). We observed no difference in size (Fig. 1*C*, one-way ANOVA, $F_{2,\ 13} = 1.306$, $P = 0.3043$) or zeta-potential (Fig. 1*D*, one-way ANOVA, $F_{2,\ 13} = 0.6167$, $P = 0.5548$) of isolated EVs. PCA plots considering all EV characteristics simultaneously detected significant separation of groups (Fig. 1*E*, PERMANOVA, main effect of group, $F = 2.6044$, $R^2 = 0.28606$, $P < 0.05$). Supplementary analyses showed no effect of dam weight or litter size on EV characteristic outcomes (Supplemental Fig. S1, *A* and *B*).

Next, to examine potential functional and signaling cargo differences of EVs isolated at these distinct reproductive time points, we used an unbiased proteomic analysis of isolated EVs. Following data processing, a total of 692 proteins were detected and included in further analyses. Functional enrichment analysis using the STRING database for all detected proteins indicated enrichment for expected EV protein functions, including Cellular Component GO terms, such as extracellular matrix, extracellular space, complement activation, and proteasome complex (Supplemental Fig. S1*C*). PCA plots that included all three groups detected significant separation between groups, suggesting distinct proteomic profiles for each (Fig. 1*F*, PERMANOVA, main effect of group, $F = 4.758$, $R^2 = 0.42263$, $P < 0.01$). To further explore proteomic differences, we made individual group comparisons (Figs. 2, 3, and 4). When comparing pregnant to nonpregnant mice, we detected 28 differentially expressed proteins, with nine upregulated and 19 downregulated in pregnant animals (Fig. 2*B*, Supplemental Table S2). Interestingly, when comparing pregnant and postpartum proteins, we detected many more differences, with 46 differentially expressed proteins, 42 upregulated and four downregulated in pregnant compared with postpartum mice (Fig. 3*B*, Supplemental Table S3). Finally, when comparing nonpregnant and postpartum mice, we detected 42 differentially expressed proteins, with three upregulated and 39 downregulated in postpartum compared with nonpregnant (Fig. 4*B*, Supplemental Table S4).

To examine the potential relevance of these protein differences, we ran a functional enrichment analysis for each comparison using the STRING database (Figs. 2*C*, 3*C*, and 4*C*) (30). To better visualize groups of proteins functionally coexpressed in signaling pathways, we used a k-means clustering algorithm with associated Biological Process GO terminology (Figs. 2*D*, 3*D*, and 4*D*) (31, 32). Comparing EVs from nonpregnant and pregnant mice, we observed in the mouse protein-protein interaction (PPI) network, two protein clusters associated with innate immune function and one cluster associated with placental protein and prolactin receptor function (Fig. 2, *C* and *D*). Comparing differentially expressed proteins between pregnant and postpartum mice, we observed one large cluster associated with plasma lipoprotein regulation, one cluster associated with extracellular matrix and cell-cell interaction, and one cluster associated with placental protein and prolactin receptor signaling

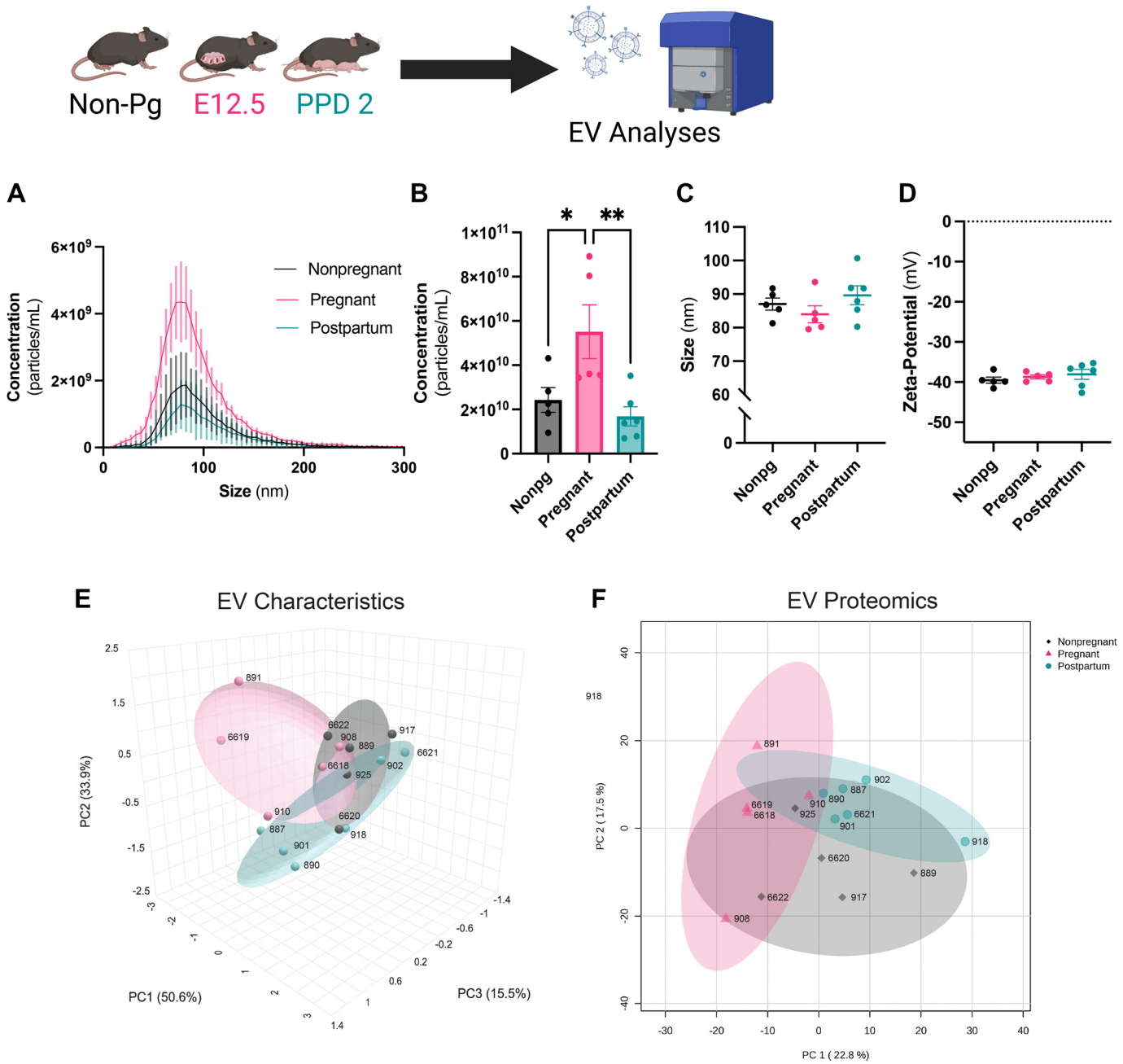

Figure 1. Maternal circulating EV concentrations increase significantly during pregnancy and return to nonpregnant levels by *postpartum day 2* but retain distinct proteomic signatures across time points. EVs were isolated from age-matched female mice ($n = 5$/group). Nanoparticle tracking analysis of EV characteristics showed increased circulating EVs in pregnant mice by (*A*) size distribution and (*B*) concentration (particles/mL) ($F_{2, 13} = 6.752$, $P < 0.01$), but no difference in (*C*) median size (nm) ($F_{2, 13} = 1.306$, $P = 0.3043$) or (*D*) zeta-potential (mV) ($F_{2, 13} = 0.6167$, $P = 0.5548$). These three EV characteristics were considered together and plotted in a (*E*) 3-D PC plot where significant separation by group was detected ($F = 2.6044$, $P = 0.044$). *F*: proteomic analysis performed on detected proteins from isolated EVs and visualized in a PCA score plot displayed significant clustering and separation between all three groups ($F = 4.758$, $P = 0.009$). Data are displayed as means ± SE; $^*P < 0.05$, $^{**}P < 0.01$. Figure, in part, created with a licensed version of BioRender.com. EV, extracellular vesicle.

(Fig. 3, *C* and *D*). Finally, comparing differentially expressed proteins between nonpregnant and postpartum mice, we found one large cluster associated with extracellular matrix organization, tissue remodeling, and general cell structure, and one small cluster associated with inflammatory signaling lipid mediators (Fig. 4, *C* and *D*).

Chemogenic Activation through DREADDs in the Placenta of Pregnant Dams Increase Concentration of Circulating EVs Relative to Wild-Type Controls

With our observation of increased EVs in our pregnancy group compared with nonpregnant and postpartum groups paired with distinct proteomic signatures (Figs. 1, 2, and 4),

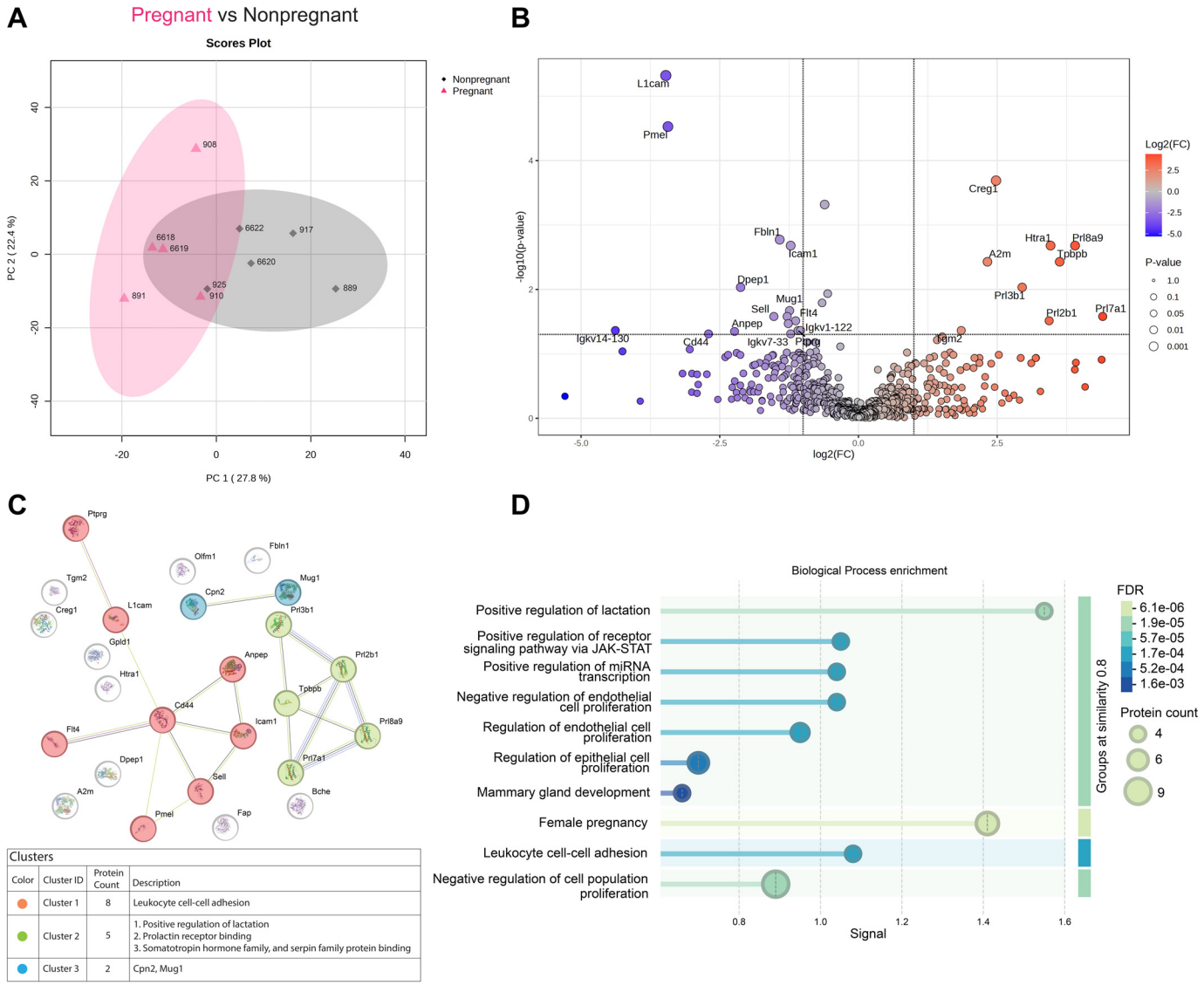

Figure 2. Unbiased functional proteomic analyses comparing pregnant and nonpregnant mice show distinct proteome signatures related to prolactin regulation and the immune system. *A*: PCA score plot based on detected EV proteins indicated significant separation between pregnant and nonpregnant, same-aged females ($F = 4.491$, $P < 0.05$). *B*: volcano plot of differentially expressed proteins indicated upregulation of nine proteins and downregulation of 19 proteins in pregnant compared with nonpregnant mice with parameters set at an FDR Q-value ≤ 0.05 and $|\log2FC| \geq 0.2$. *C*: predicted protein-protein interactions and cluster analysis of differentially expressed proteins using a k-means clustering algorithm and the STRING database indicated three significant clusters, with two related to the immune system and one related to prolactin regulation. Color of node indicates cluster identity and number of lines connecting nodes indicates predicted strength of interaction between two proteins. *D*: functional enrichment of differentially expressed proteins based on biological process GO terminology indicated strong associations with terms describing regulation of lactation and the immune system. Size of circles indicates the number of differentially expressed proteins annotated with a particular term. False discovery rate (FDR) indicated by color describes how significant a particular enrichment is using the Benjamini–Hochberg procedure. Signal is a weighted harmonic mean between the observed/expected ratio and −log(FDR). EV, extracellular vesicle.

we used a dynamic in vivo model to further explore the role EVs, specifically released by the placenta, play during pregnancy. Using a transgenic mouse model through breeding Cyp19.Cre+ (P.Cre) mice with DRD+ mice to express the metabotropic Gq-DREADD receptor specifically in placental cells of trophoblast origin, we activated the secretory pathway of trophoblast cells to elicit an increase in extracellular vesicles in maternal circulation. At E15.5, when we administered CNO through intraperitoneal injection of 1 mg/kg, we demonstrated a significant increase in maternal circulating EVs in DRD+ mice relative to wild-type controls (Fig. 5, *A* and *B*, two-tailed *t* test, $t_7 = 3.021$, $P < 0.05$). We did not observe significant differences in EV size (Fig. 5*C*, two-tailed *t* test, $t_7 = 1.420$, $P = 0.1985$) or zeta-potential (Fig. 5*D*, two-tailed *t* test, $t_7 = 1.343$, $P = 0.2212$). Additional analyses demonstrated no significant effect on EV concentration due to other factors, including litter size, litter sex composition, and maternal body weight (Supplemental Fig. S2, *A*–*C*). To probe if the resulting increase of maternal circulating EVs after CNO administration may have preferentially secreted a specific EV subtype, we performed Western blots to detect the presence of proteins associated with EV subtypes, CD9

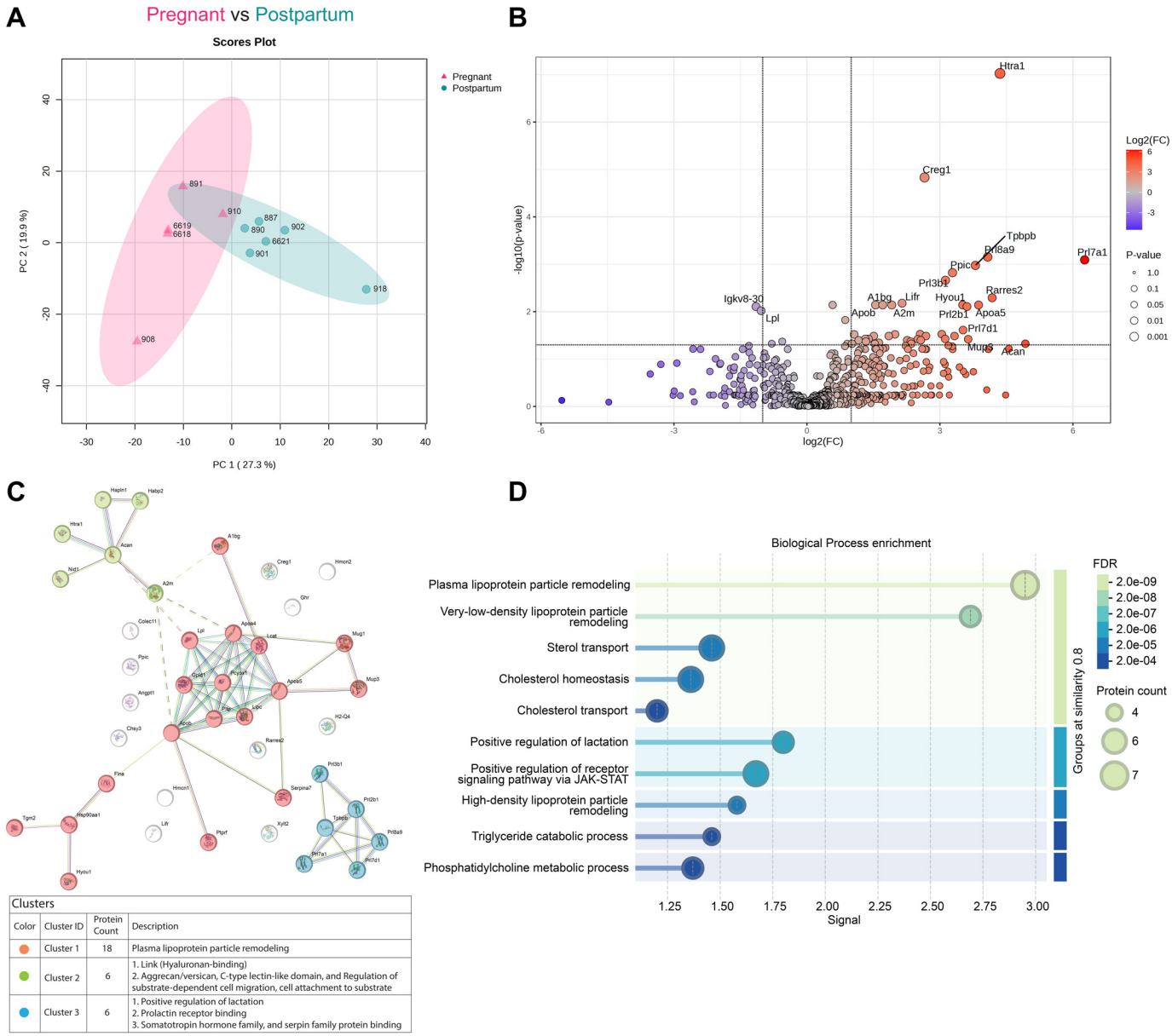

Clusters

Color	Cluster ID	Protein Count	Description
	Cluster 1	18	Plasma lipoprotein particle remodeling
	Cluster 2	6	1. Link (Hyaluronan-binding) 2. Aggrecan/versican, C-type lectin-like domain, and Regulation of substrate-dependent cell migration, cell attachment to substrate
	Cluster 3	6	1. Positive regulation of lactation 2. Prolactin receptor binding 3. Somatotropin hormone family, and serpin family protein binding

Figure 3. Unbiased functional proteomic analyses comparing pregnant and postpartum mice show distinct proteome signatures related to regulation of lipoproteins, lactation, and the immune system. *A*: PCA score plot based on detected EV proteins indicated significant separation between pregnant and postpartum mice ($F = 5.7113$, $P < 0.01$). *B*: volcano plot of differentially expressed proteins indicated upregulation of 46 proteins and downregulation of four proteins in pregnant mice with parameters set at an FDR Q-value ≤ 0.05 and $|\log2FC| \geq 0.2$. *C*: predicted protein-protein interactions and cluster analysis of differentially expressed proteins using a k-means clustering algorithm and the STRING database indicated three significant clusters with one related to lipoprotein particle structure, one related to cell migration and adhesion processes, and one related to prolactin and prolactin receptor regulation. Color of node indicates cluster identity and number of lines connecting nodes indicates the predicted strength of interaction between two proteins. *D*: functional enrichment of differentially expressed proteins based on biological process GO terminology indicated strong association with terms related to lipoprotein, lactation, and immune system regulation. Size of circles indicates the number of differentially expressed proteins annotated with a particular term. False discovery rate (FDR) indicated by color describes how significant a particular enrichment is using the Benjamini–Hochberg procedure. Signal is a weighted harmonic mean between the observed/expected ratio and −log(FDR). EV, extracellular vesicle.

for exosomes and Annexin A2 (ANXA2) for microvesicles. We observed higher amounts of CD9 protein in EVs isolated from DRD+ maternal circulation compared with WT controls (Fig. 5*E*). To further explore if the EVs released after CNO administration may have unique functional signaling cargo, we performed proteomic analysis. PCA plots (Fig. 5*F*, PERMANOVA, main effect of group, $F = 1.3723$, $R^2 = 0.14642$, $P = 0.299$) and t tests of individual detected proteins did not detect significant differences in proteomic composition between isolated circulating EVs from DRD+ and WT dams (Fig. 5*G*).

CNO Activation of DREADDs in the Placenta of Pregnant Dams Impacts Glucose Dynamics

As we demonstrated, we could elicit an increase in EV concentration quickly after activating the placental secretory

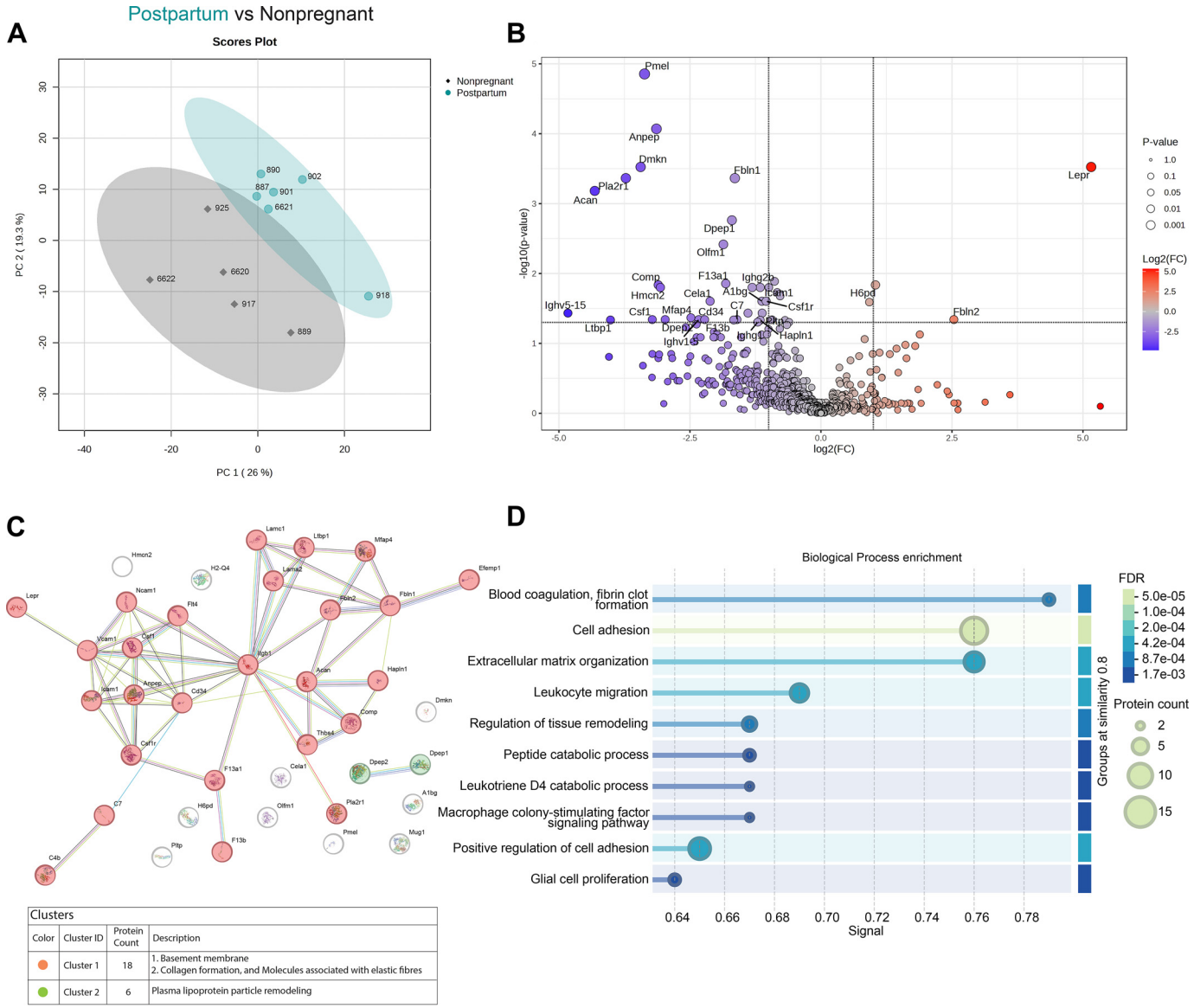

Figure 4. Unbiased functional proteomic analysis comparing postpartum and nonpregnant mice shows distinct proteome signatures related to extracellular matrix and tissue organization and regulation of the immune system. *A*: PCA score plot based on detected EV proteins indicated significant separation between nonpregnant and postpartum animals ($F = 6.1708$, $P < 0.01$). *B*: volcano plot of differentially expressed proteins indicated three upregulated and 39 downregulated proteins in postpartum compared with nonpregnant mice with parameters set at an FDR Q-value ≤ 0.05 and $|\log2FC| \geq 0.2$. *C*: predicted protein-protein interactions and cluster analysis of differentially expressed proteins using a k-means clustering algorithm and the STRING database indicated two clusters, with the one large cluster associated with extracellular and tissue organization and one smaller cluster associated with leukotriene catabolism. Color of node indicates cluster identity and number of lines connecting nodes indicates predicted strength of interaction between two proteins. *D*: functional enrichment of differentially expressed proteins based on biological process GO terminology indicated strong association with terms related to extracellular matrix and tissue remodeling and immune system regulation. Size of circles indicates the number of differentially expressed proteins annotated with a particular term. False discovery rate (FDR) indicated by color describes how significant a particular enrichment is using the Benjamini–Hochberg procedure. Signal is a weighted harmonic mean between the observed/expected ratio and −log(FDR). EV, extracellular vesicle.

pathway with CNO administration (Fig. 5, *A* and *B*), we therefore wanted to test the functional impact of these EVs in a dynamic homeostatic process known to be impacted during pregnancy, such as glucose regulation. We tested this through simultaneously stimulating the placental secretory pathway with our chemogenetic model and performing a glucose tolerance test (GTT). We observed a reduced ability to clear glucose from circulation in our DRD+ mice compared with WT controls (Fig. 5*H*). Although we did not detect a significant difference in area under the curve between the two groups (Supplemental Fig. S2*E*, two-tailed *t* test, $t_{13} = 1.372$, $P = 0.1931$), when we examined the glucose recovery slope from the peak of circulating glucose (30 min) to the final measure of glucose levels (120 min), there was a significant reduction in slope in the DRD+ mice (Fig. 5*I*, two-tailed *t* test, $t_{13} = 2.502$, $P < 0.05$). Of note, when the percentage of pups in the litter that expressed both P.Cre and DRD

genotypes was plotted against glucose area under the curve, we observed a positive linear correlation (Fig. 5*J*, $R^2 = 0.414$). Individual traces of GTT curves showed larger intergroup variance in DRD+ mice compared with WT mice (Fig. 5, *K* and *L*). Supplemental analyses showed litter size, sex ratio of the litter, and dam body weight all appeared not to influence the glucose area under the curve (Supplemental Fig. S2, *F*–*H*).

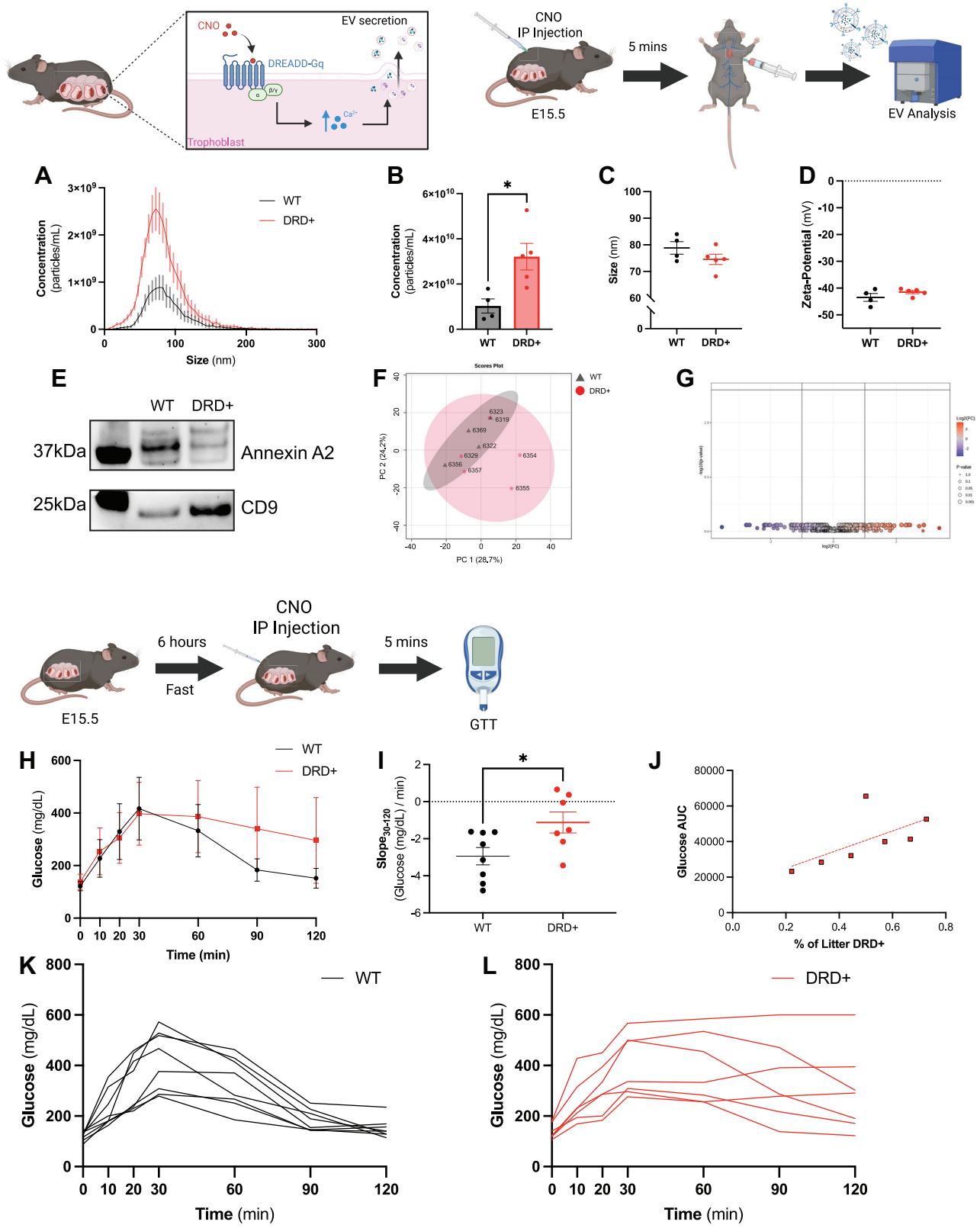

AJP-Endocrinol Metab • doi:10.1152/ajpendo.00061.2026

DISCUSSION

Maintenance of homeostasis during pregnancy is a dynamic and metabolically demanding process that substantially impacts maternal health (3, 5, 33, 34). The placenta plays a crucial role in coordinating communication and signaling in maternal circulation, in part, through secretion of extracellular vesicles (EVs) (8, 10, 11). The diverse roles EVs perform during pregnancy are currently being fully elucidated, but include critical homeostatic functions involved with immune and glucose regulation (7, 8, 12, 35–39). Understanding the dynamic changes in EVs across pregnancy and postpartum periods is a valuable step in identifying potential novel diagnostic and therapeutic biomarkers in improving maternal health (11).

In our preclinical mouse study, we first examined key characteristic differences in EVs from maternal circulation, comparing changes that occur in pregnancy and postpartum. As hypothesized and previously shown, EVs were significantly increased in concentration during pregnancy compared with nonpregnant and postpartum groups (19, 40). These findings match previous work in human studies that demonstrated significant increases, up to 3–4 times higher, in circulating EV concentration during pregnancy (13, 14). Although we predicted EV concentration in the postpartum period would be reduced relative to pregnancy, we were surprised to find a significant reduction back to that of nonpregnant levels, suggesting a rapid removal of circulating EVs following loss of the placenta at parturition. Such a dramatic loss of key homeostatic and regulatory capacity provided by circulating EVs may be an important focus for future studies examining health challenges in women unique to the postpartum period (41). We note that our studies here were completed in healthy, nonchallenged female mice living in a clean environment and on a healthy standard chow diet high in soluble fiber and low in fat (42). More dramatic changes may be found in studies where stress or other challenges are included.

Although identifying changes in EV characteristics is informative, examination of EV functional cargo provides an additional level of insight for reproductive system and pathway engagement (8, 9, 43, 44). Previous studies reported that EV miRNA cargo changed throughout pregnancy to meet dynamic regulatory demands (45). Although miRNAs packaged into EVs in circulation come from numerous tissue sources, EV protein cargo, especially in microvesicle subtypes of EVs blebbed from the cell membrane, can be highly informative as to cell type or tissue of origin (46, 47). Here, we expanded knowledge in this field through using unbiased examination of protein cargo associated with circulating EVs across reproductive states. Our analyses revealed unique EV proteomic signatures across the nonpregnant, pregnant, and postpartum states. For example, EVs isolated from pregnant mice had significantly increased proteins specific to placental function or to cell mechanisms known to be essential for placental development, including trophoblast-specific protein beta (Tpbpb), a mouse gene crucial for placental development and specifically expressed in the junctional zone of the placenta, and cellular repressor of E1A-stimulated genes 1 (Creg1) that plays a vital role in pregnancy, specifically in placental development by promoting trophoblast cell proliferation, differentiation, and EV release (48, 49). Although not surprising, this finding validates our hypothesis that the placenta significantly contributes to the increased circulating EV concentration. In addition, we found that the L1 cell adhesion molecule (L1CAM), a transmembrane glycoprotein expressed in neuron cell membranes and important in immune control of leukocyte trafficking, was dramatically decreased in EVs in pregnancy. Although L1CAM has been frequently interpreted as a circulating biomarker for EVs of neural origin, current evidence suggests it is also important for immune cell communication and is abundant as a secreted protein in circulation (50, 51). We also detected significantly increased prolactin protein family members, including Prl2b1, Prl3b1, Prl7a1, and Prl8a9, in EVs from pregnant mice. Previous studies reported that prolactin and prolactin receptor signaling during pregnancy are important regulators of insulin release and may be involved in the development of insulin resistance throughout pregnancy (52–57). Although an increase in prolactin proteins during pregnancy is not surprising, a functional role for them specific to EV communication has not been elucidated (58–60).

An additional outcome from our study is the important and novel finding that while the concentration of maternal circulating EVs was similar between nonpregnant and postpartum mice, our analysis found significant differences in their EV protein composition. EVs from postpartum mice showed strong pathway association and enrichment for proteins associated with extracellular matrix and tissue organization that may reflect the homeostatic maternal demands soon after birth. Interestingly, one of the few proteins showing robust increased levels in EVs unique to the postpartum period was the leptin receptor. EV leptin receptors can bind to circulating leptin and transfer signals to target cells, influencing placental function and the maternal immune system and metabolism (61–64). Of note, in this study, we examined

Figure 5. Dynamic increases in circulating EVs using chemogenetic activation of the placental secretory pathway significantly impacts maternal glucose regulation during pregnancy. EVs were isolated from age-matched E15.5 pregnant mice who were either wild type (WT, black lines/dots) or DREADD + (DRD +, red lines/dots). Nanotracking particle analysis of EVs characteristics 5 mins after CNO (1 mg/kg) administration demonstrated an increase in circulating EVs from DRD + mice by (*A*) size distribution and (*B*) concentration (particles/mL) ($t_7 = 3.021$, $P = 0.0194$), but not (*C*) median size ($t_7 = 1.420$, $P = 0.1985$) or (*D*) zeta-potential ($t_7 = 1.343$, $P = 0.2212$). *E*: representative Western blot images of isolated EVs were captured using EV-specific antibodies CD9 and Annexin A2 (ANXA2) suggesting increased CD9 and reduced ANXA2 expression in DRD + mice. Proteomic analysis of EVs was visualized with (*F*) principal component analysis (PCA) score plots ($F = 1.277$, $P = 0.361$), and (*G*) volcano plots indicated no significantly differentially expressed proteins in DRD + mice compared with WT mice. *H*: glucose tolerance curves for WT and DRD + animals after receiving 1 mg/kg CNO injection 5 mins before the glucose tolerance test suggested a reduced ability of DRD + animals to clear circulating glucose [$F_{time*genotype}$ (2.870, 37.31) = 5.366, $P = 0.004$]. *I*: slope analysis of glucose curves from peak glucose at 30 mins to end time point at 120 mins demonstrated a significantly reduced slope in DRD + mice ($t_{13} = 2.502$, $P = 0.0265$). *J*: glucose area under the curve (AUC) demonstrates a positive linear relationship with the percentage of the litter that expresses DRD + genotype ($R^2 = 0.4140$). Individual glucose curves for (*K*) wildtype and (*L*) DRD + animals after receiving 1 mg/kg CNO injection 5 mins before the glucose tolerance test demonstrated increased intergroup variability in DRD + mice. Data are displayed as means ± SE; $^*P < 0.05$. Figure, in part, created with a licensed version of BioRender.com. CNO, clozapine-*N*-oxide; EV, extracellular vesicle.

EVs from mice 48 h after parturition, an acute postpartum time frame. EV cargo is likely influenced by lactation hormones and is expected to be distinct at later postpartum time points.

Previous studies by our group and others connected EV signaling during pregnancy with glucose regulation using mouse tail vein injection of maternal EVs isolated in pregnancy (6, 19, 65). However, it remains unclear whether placental EVs specifically contribute to glucose homeostasis. Therefore, we applied a novel chemogenetic approach using DREADD (DRD+) transgenic mice to activate the secretory pathway in trophoblast-derived cells to dynamically increase maternal circulating EVs and measured changes in maternal glucose following CNO administration during a glucose challenge. We confirmed a rapid and significant increase in circulating EV concentration in DRD+ mice following CNO, but no significant changes in average EV size or zeta potential were observed. Using biochemical assessment of standard EV subtype markers, we found a potential increase in CD9-positive exosomes and a reduction in annexin A2-positive microvesicles. Although this was unexpected, as Gq-DREADD activation increases intracellular calcium and would predict increased microvesicle secretion, we also observed a similar indication of EV size change toward smaller EVs (66, 67). EV subtypes, such as exosomes and microvesicles, perform unique roles in cell-to-cell communication and in acute response to stimuli, as well as longer-term chronic maintenance of homeostasis (68–70). To determine if the EV protein cargo changed in DRD+ mice, we performed unbiased proteomic analyses. Interestingly, while we significantly increased the concentration of circulating EVs in DRD+ mice, we did not find significant differences in proteins detected or their relative abundance, suggesting we were able to manipulate circulating EV secretion without distorting the detectable protein composition. These results suggest that the placenta may be capable of dynamic EV secretion to control maternal homeostasis.

During pregnancy progression, reduced maternal glucose sensitivity occurs and circulating EV concentrations also rise substantially (33, 71, 72). However, the ability for placental EVs to function as dynamic homeostatic regulators of glucose sensitivity in pregnancy is less clear. Using our chemogenetic approach, we examined how a dynamic increase in circulating EVs following CNO treatment could alter responses to a maternal glucose challenge. We found a reduction in maternal ability to clear glucose in DRD+ mice, with a significant reduction in the slope of glucose recovery. Interestingly, we also noted in the DRD+ mice an increased intragroup variance relative to wild-type mice. The increased variability and increased glucose area under the curve demonstrated a positive association with the percentage of the DRD+ placenta within the litter (i.e., placenta that expressed both P.Cre+ and DRD+ genotypes), supporting a causal role for DRD+ placental increases in EV secretion to alter maternal glucose sensitivity. Interestingly, in gestational diabetes (GDM), maternal EV concentrations are significantly increased, suggesting that EVs may be either attempting to compensate for the glucose dysregulation or play a role in GDM development, or both (65). Furthermore, recent studies found that EVs isolated from the media of chorionic villi explants modulated glucose uptake of skeletal myocytes in culture (17). Our previous work showed similar support for a role of EVs in glucose homeostasis in pregnancy, where EVs from pregnant dams injected into nonpregnant mice altered glucose dynamics (19). However, it is important to note that pregnant EVs acting in a nonpregnant setting are unlikely to replicate the highly unique hormonal milieu characteristic of pregnancy. Together, these data support an ability for circulating EVs to serve an important role in maternal glucose regulation, and that disruption to this normal function, such as demonstrated in our chemogenetic model, could result in increased risk for gestational diabetes or other metabolic disorders. Although the target tissue or site(s) of EV action (e.g., skeletal muscle, liver, pancreas, etc.) remain less clear, future studies could investigate this important question.

A major strength of these studies is the novel identification of distinct changes in EV protein cargo across pregnancy and postpartum using unbiased proteomic analyses, suggesting unique EV functions. The development of a chemogenetic approach to dynamically control the placenta secretory pathway also provides insight into specific roles of placental EVs in maternal homeostasis. We note several limitations in these studies that could be focused on in future studies, including the recognition that our data are assessed from a single time point in pregnancy and postpartum and may not reflect all changes in EV function across these periods. Furthermore, in our chemogenetic approach, stimulation of the calcium-mediated secretory pathway in trophoblast cells likely secretes additional proteins and components into maternal circulation that are not limited to EVs. This is especially important when interpreting functional readouts of glucose dynamics, as some factors such as placental lactogens are known to influence maternal glucose regulation (73, 74). Future studies using this approach could consider characterization of these additional factors in circulation following CNO stimulation.

In summary, the data demonstrate distinct changes in circulating EV protein cargo across pregnancy and the postpartum period, revealing a unique proteomic signature that is independent of EV concentration changes. As EV proteins can point to novel cell and tissue engagement, these data may provide insight into maternal systems and processes specific to reproductive timing. As such, these results build upon previous work and support the importance of EVs as potential biomarkers in maternal health.

DATA AVAILABILITY

Data will be made available from the corresponding author upon reasonable request.

SUPPLEMENTAL MATERIAL

Supplemental Figs. S1 and S2 and Supplemental Tables S1–S4: https://doi.org/10.6084/m9.figshare.31310176.

ACKNOWLEDGMENTS

The graphical abstract and Figs. 1 and 5 were created, in part, with a licensed version of BioRender.com.

GRANTS

This research was supported by National Institute of Child Health and Human Development (NICHD) 5R01HD097093-06, 1R01HD117700-01 (to T.L.B.), and 5T32HD007186-45.

DISCLOSURES

No conflicts of interest, financial or otherwise, are declared by the authors.

AUTHOR CONTRIBUTIONS

G.A.D. and T.L.B. conceived and designed research; G.A.D. and R.O. performed experiments; G.A.D. analyzed data; G.A.D., A.S.F., R.O., and T.L.B. interpreted results of experiments; G.A.D. prepared figures; G.A.D. and T.L.B. drafted manuscript; G.A.D., A.S.F., R.O., and T.L.B. edited and revised manuscript; G.A.D., A.S.F., R.O., and T.L.B. approved final version of manuscript.

REFERENCES

1. **Pregnancy Mortality Surveillance System.** Maternal and Infant Health | CDC (Online). 2023. [2024 Apr 30]. https://www.cdc.gov/reproductivehealth/maternal-mortality/pregnancy-mortality-surveillance-system.htm.
2. **Diaz-Santana MV**, **O'Brien KM**, **Park Y-MM**, **Sandler DP**, **Weinberg CR.** Persistence of risk for type 2 diabetes after gestational diabetes mellitus. *Diabetes Care* 45: 864–870, 2022. doi:10.2337/dc21-1430.
3. **Perng W**, **Stuart J**, **Rifas-Shiman SL**, **Rich-Edwards JW**, **Stuebe A**, **Oken E.** Preterm birth and long-term maternal cardiovascular health. *Ann Epidemiol* 25: 40–45, 2015. doi:10.1016/j.annepidem.2014.10.012.
4. **Swart T**, **Shandley K**, **Huynh M**, **Brown CM**, **Austin DW**, **Bhowmik J.** Pregnancy complications and their association with postpartum depression symptoms: a retrospective study. *Aust J Psychol* 75: 2247088, 2023. doi:10.1080/00049530.2023.2247088.
5. **Turbeville HR**, **Sasser JM.** Preeclampsia beyond pregnancy: long-term consequences for mother and child. *Am J Physiol Renal Physiol* 318: F1315–F1326, 2020. doi:10.1152/ajprenal.00071.2020.
6. **James-Allan LB**, **Rosario FJ**, **Barner K**, **Lai A**, **Guanzon D**, **McIntyre HD**, **Lappas M**, **Powell TL**, **Salomon C**, **Jansson T.** Regulation of glucose homeostasis by small extracellular vesicles in normal pregnancy and in gestational diabetes. *FASEB J* 34: 5724–5739, 2020. doi:10.1096/fj.201902522RR.
7. **Mincheva-Nilsson L.** Immunosuppressive protein signatures carried by syncytiotrophoblast-derived exosomes and their role in human pregnancy. *Front Immunol* 12: 717884, 2021. doi:10.3389/fimmu.2021.717884.
8. **Morelli AE**, **Sadovsky Y.** Extracellular vesicles and immune response during pregnancy: a balancing act. *Immunol Rev* 308: 105–122, 2022. doi:10.1111/imr.13074.
9. **Nakahara A**, **Nair S**, **Ormazabal V**, **Elfeky O**, **Garvey CE**, **Longo S**, **Salomon C.** Circulating placental extracellular vesicles and their potential roles during pregnancy. *Ochsner J* 20: 439–445, 2020. doi:10.31486/toj.20.0049.
10. **Ouyang Y**, **Bayer A**, **Chu T**, **Tyurin VA**, **Kagan VE**, **Morelli AE**, **Coyne CB**, **Sadovsky Y.** Isolation of human trophoblastic extracellular vesicles and characterization of their cargo and antiviral activity. *Placenta* 47: 86–95, 2016. doi:10.1016/j.placenta.2016.09.008.
11. **Sadovsky Y**, **Ouyang Y**, **Powell JS**, **Li H**, **Mouillet J-F**, **Morelli AE**, **Sorkin A**, **Margolis L.** Placental small extracellular vesicles: current questions and investigative opportunities. *Placenta* 102: 34–38, 2020. doi:10.1016/j.placenta.2020.03.002.
12. **Tannetta D**, **Dragovic R**, **Alyahyaei Z**, **Southcombe J.** Extracellular vesicles and reproduction–promotion of successful pregnancy. *Cell Mol Immunol* 11: 548–563, 2014. doi:10.1038/cmi.2014.42.
13. **Salomon C**, **Torres MJ**, **Kobayashi M**, **Scholz-Romero K**, **Sobrevia L**, **Dobierzewska A**, **Illanes SE**, **Mitchell MD**, **Rice GE.** A gestational profile of placental exosomes in maternal plasma and their effects on endothelial cell migration. *PLoS One* 9: e98667, 2014. doi:10.1371/journal.pone.0098667.
14. **Sarker S**, **Scholz-Romero K**, **Perez A**, **Illanes SE**, **Mitchell MD**, **Rice GE**, **Salomon C.** Placenta-derived exosomes continuously increase in maternal circulation over the first trimester of pregnancy. *J Transl Med* 12: 204, 2014. doi:10.1186/1479-5876-12-204.
15. **Chang X**, **Yao J**, **He Q**, **Liu M**, **Duan T**, **Wang K.** Exosomes from women with preeclampsia induced vascular dysfunction by delivering sFlt (soluble Fms-like tyrosine kinase)-1 and sEng (Soluble Endoglin) to endothelial cells. *Hypertension* 72: 1381–1390, 2018. doi:10.1161/HYPERTENSIONAHA.118.11706.
16. **Kurian NK**, **Modi D.** Extracellular vesicle mediated embryo-endometrial cross talk during implantation and in pregnancy. *J Assist Reprod Genet* 36: 189–198, 2019. doi:10.1007/s10815-018-1343-x.
17. **Nair S**, **Jayabalan N**, **Guanzon D**, **Palma C**, **Scholz-Romero K**, **Elfeky O**, **Zuñiga F**, **Ormazabal V**, **Diaz E**, **Rice GE**, **Duncombe G**, **Jansson T**, **McIntyre HD**, **Lappas M**, **Salomon C.** Human placental exosomes in gestational diabetes mellitus carry a specific set of miRNAs associated with skeletal muscle insulin sensitivity. *Clin Sci (Lond)* 132: 2451–2467, 2018. doi:10.1042/CS20180487.
18. **Sheller-Miller S**, **Trivedi J**, **Yellon SM**, **Menon R.** Exosomes cause preterm birth in mice: evidence for paracrine signaling in pregnancy. *Sci Rep* 9: 608, 2019. doi:10.1038/s41598-018-37002-x.
19. **Zierden HC**, **Marx-Rattner R**, **Rock KD**, **Montgomery KR**, **Anastasiadis P**, **Folts L**, **Bale TL.** Extracellular vesicles are dynamic regulators of maternal glucose homeostasis during pregnancy. *Sci Rep* 13: 4568, 2023. doi:10.1038/s41598-023-31425-x.
20. **Verweij FJ**, **Bebelman MP**, **Jimenez CR**, **Garcia-Vallejo JJ**, **Janssen H**, **Neefjes J**, **Knol JC**, **de Goeij-de Haas R**, **Piersma SR**, **Baglio SR**, **Verhage M**, **Middeldorp JM**, **Zomer A**, **van Rheenen J**, **Coppolino MG**, **Hurbain I**, **Raposo G**, **Smit MJ**, **Toonen RFG**, **van Niel G**, **Pegtel DM.** Quantifying exosome secretion from single cells reveals a modulatory role for GPCR signaling. *J Cell Biol* 217: 1129–1142, 2018. doi:10.1083/jcb.201703206.
21. **Elmore SA**, **Cochran RZ**, **Bolon B**, **Lubeck B**, **Mahler B**, **Sabio D**, **Ward JM.** Histology atlas of the developing mouse placenta. *Toxicol Pathol* 50: 60–117, 2022. doi:10.1177/01926233211042270.
22. **Wenzel PL**, **Leone G.** Expression of Cre recombinase in early diploid trophoblast cells of the mouse placenta. *Genesis* 45: 129–134, 2007. doi:10.1002/dvg.20276.
23. **Morgan CP**, **Meadows VE**, **Marx-Rattner R**, **Cisse YM**, **Bale TL.** HA-tag CD63 is a novel conditional transgenic approach to track extracellular vesicle interactions with sperm and their transfer at conception. *Sci Rep* 13: 707, 2023. doi:10.1038/s41598-023-27898-5.
24. **Everman JL**, **Sajuthi SP**, **Liegeois MA**, **Jackson ND**, **Collet EH**, **Peters MC**, **et al.** A common polymorphism in the Intelectin-1 gene influences mucus plugging in severe asthma. *Nat Commun* 15: 3900, 2024. doi:10.1038/s41467-024-48034-5.
25. **Van Hove JLK**, **Friederich MW**, **Hock DH**, **Stroud DA**, **Caruana NJ**, **Christians U**, **Schniedewind B**, **Michel CR**, **Reisdorph R**, **Lopez Gonzalez EDJ**, **Brenner C**, **Donovan TE**, **Lee JC**, **Chatfield KC**, **Larson AA**, **Baker PR**, **McCandless SE**, **Moore Burk MF.** ACAD9 treatment with bezafibrate and nicotinamide riboside temporarily stabilizes cardiomyopathy and lactic acidosis. *Mitochondrion* 78: 101905, 2024. doi:10.1016/j.mito.2024.101905.
26. **Demichev V**, **Messner CB**, **Vernardis SI**, **Lilley KS**, **Ralser M.** DIA-NN: neural networks and interference correction enable deep proteome coverage in high throughput. *Nat Methods* 17: 41–44, 2020. doi:10.1038/s41592-019-0638-x.
27. **Kistner F**, **Grossmann JL**, **Sinn LR**, **Demichev V.** QuantUMS: uncertainty minimisation enables confident quantification in proteomics (Preprint). *bioRxiv*, 2023. doi:10.1101/2023.06.20.545604v1.
28. **Pang Z**, **Lu Y**, **Zhou G**, **Hui F**, **Xu L**, **Viau C**, **Spigelman AF**, **MacDonald PE**, **Wishart DS**, **Li S**, **Xia J.** MetaboAnalyst 6.0: towards a unified platform for metabolomics data processing, analysis and interpretation. *Nucleic Acids Res* 52: W398–W406, 2024. doi:10.1093/nar/gkae253.
29. **Garrido-Martín D**, **Calvo M**, **Reverter F**, **Guigó R.** A fast non-parametric test of association for multiple traits. *Genome Biol* 24: 230, 2023. doi:10.1186/s13059-023-03076-8.
30. **Szklarczyk D**, **Kirsch R**, **Koutrouli M**, **Nastou K**, **Mehryary F**, **Hachilif R**, **Gable AL**, **Fang T**, **Doncheva NT**, **Pyysalo S**, **Bork P**, **Jensen LJ**, **von Mering C.** The STRING database in 2023: protein-protein association networks and functional enrichment analyses for any

sequenced genome of interest. *Nucleic Acids Res* 51: D638–D646, 2023. doi:10.1093/nar/gkac1000.
31. **Aleksander SA**, **Balhoff J**, **Carbon S**, **Cherry JM**, **Drabkin HJ**, **Ebert D**, **et al.** The Gene Ontology knowledgebase in 2023. *Genetics* 224: iyad031, 2023. doi:10.1093/genetics/iyad031.
32. **Ashburner M**, **Ball CA**, **Blake JA**, **Botstein D**, **Butler H**, **Cherry JM**, **Davis AP**, **Dolinski K**, **Dwight SS**, **Eppig JT**, **Harris MA**, **Hill DP**, **Issel-Tarver L**, **Kasarskis A**, **Lewis S**, **Matese JC**, **Richardson JE**, **Ringwald M**, **Rubin GM**, **Sherlock G.** Gene Ontology: tool for the unification of biology. *Nat Genet* 25: 25–29, 2000. doi:10.1038/75556.
33. **Barbour LA**, **McCurdy CE**, **Hernandez TL**, **Kirwan JP**, **Catalano PM**, **Friedman JE.** Cellular mechanisms for insulin resistance in normal pregnancy and gestational diabetes. *Diabetes Care* 30: S112–S119, 2007. doi:10.2337/dc07-s202.
34. **Reece EA.** The fetal and maternal consequences of gestational diabetes mellitus. The. *J Matern Fetal Neonatal Med* 23: 199–203, 2010. doi:10.3109/14767050903550659.
35. **Kshirsagar SK**, **Alam SM**, **Jasti S**, **Hodes H**, **Nauser T**, **Gilliam M**, **Billstrand C**, **Hunt JS**, **Petroff MG.** Immunomodulatory molecules are released from the first trimester and term placenta via exosomes. *Placenta* 33: 982–990, 2012. doi:10.1016/j.placenta.2012.10.005.
36. **Rice GE**, **Scholz-Romero K**, **Sweeney E**, **Peiris H**, **Kobayashi M**, **Duncombe G**, **Mitchell MD**, **Salomon C.** The effect of glucose on the release and bioactivity of exosomes from first trimester trophoblast cells. *J Clin Endocrinol Metab* 100: E1280–E1288, 2015. doi:10.1210/jc.2015-2270.
37. **Sabapatha A**, **Gercel-Taylor C**, **Taylor DD.** Specific isolation of placenta-derived exosomes from the circulation of pregnant women and their immunoregulatory consequences. *Am J Reprod Immunol* 56: 345–355, 2006. doi:10.1111/j.1600-0897.2006.00435.x.
38. **Tolosa JM**, **Schjenken JE**, **Clifton VL**, **Vargas A**, **Barbeau B**, **Lowry P**, **Maiti K**, **Smith R.** The endogenous retroviral envelope protein syncytin-1 inhibits LPS/PHA-stimulated cytokine responses in human blood and is sorted into placental exosomes. *Placenta* 33: 933–941, 2012. doi:10.1016/j.placenta.2012.08.004.
39. **Zhang J**, **Li H**, **Fan B**, **Xu W**, **Zhang X.** Extracellular vesicles in normal pregnancy and pregnancy-related diseases. *J Cell Mol Med* 24: 4377–4388, 2020. doi:10.1111/jcmm.15144.
40. **Yustinasari LR**, **Hyoto M**, **Imai H**, **Kusakabe KT.** Appearance of small extracellular vesicles in the mouse pregnant serum and the localization in placentas. *J Vet Med Sci* 86: 787–795, 2024. doi:10.1292/jvms.24-0047.
41. **Ng C**, **Szücs A**, **Goh LH.** Common maternal health problems and their correlates in early post-partum mothers. *Womens Health (Lond)* 20: 17455057241227879, 2024. doi:10.1177/17455057241227879.
42. **Morrison KE**, **Jašarević E**, **Howard CD**, **Bale TL.** It's the fiber, not the fat: significant effects of dietary challenge on the gut microbiome. *Microbiome* 8: 15, 2020. doi:10.1186/s40168-020-0791-6.
43. **Noren Hooten N**, **McFarland MH**, **Freeman DW**, **Mode NA**, **Ezike N**, **Zonderman AB**, **Evans MK.** Association of extracellular vesicle protein cargo with race and clinical markers of mortality. *Sci Rep* 9: 17582, 2019. doi:10.1038/s41598-019-53640-1.
44. **Tong M**, **Kleffmann T**, **Pradhan S**, **Johansson CL**, **DeSousa J**, **Stone PR**, **James JL**, **Chen Q**, **Chamley LW.** Proteomic characterization of macro-, micro- and nano-extracellular vesicles derived from the same first trimester placenta: relevance for feto-maternal communication. *Hum Reprod* 31: 687–699, 2016. doi:10.1093/humrep/dew004.
45. **Foley HB**, **Howe CG**, **Eckel SP**, **Chavez T**, **Gevorkian L**, **Reyes EG**, **Kapanke B**, **Martinez D**, **Xue S**, **Suglia SF**, **Bastain TM**, **Marsit C**, **Breton CV.** Extracellular vesicle-enriched miRNA profiles across pregnancy in the MADRES cohort. *PLoS One* 16: e0251259, 2021. doi:10.1371/journal.pone.0251259.
46. **Watanabe S**, **Makino T**, **Hiro K**, **Sasaki T**, **Takahashi Y**, **Futagawa K**, **Suzuki M**, **Sato R**, **Yamauchi Y.** Proteomic profiling of tissue extracellular vesicles (EVs) identifies tissue EV markers and estimates the abundance of tissue EVs in the circulation. *Extracell Vesicle* 6: 100097, 2025. doi:10.1016/j.vesic.2025.100097.
47. **Clancy JW**, **Schmidtmann M**, **D'Souza-Schorey C.** The ins and outs of microvesicles. *FASEB Bioadv* 3: 399–406, 2021. doi:10.1096/fba.2020-00127.
48. **Shalom-Barak T**, **Zhang X**, **Chu T**, **Timothy Schaiff W**, **Reddy JK**, **Xu J**, **Sadovsky Y**, **Barak Y.** Placental PPARγ regulates spatiotemporally diverse genes and a unique metabolic network. *Dev Biol*. 372: 143–155, 2012. doi:10.1016/j.ydbio.2012.08.021.
49. **Yuan N**, **Xiao L**, **Chen J**, **Liu B**, **Ren S**, **Sheng X**, **Qi X**, **Wang Y**, **Chen C**, **Guo K**, **Yang X**, **Yang L**, **Wang X.** CREG1 promotes bovine placental trophoblast cells exosome release by targeting IGF2R and participates in regulating organoid differentiation via exosomes transport. *Int J Biol Macromol* 274: 133298, 2024. doi:10.1016/j.ijbiomac.2024.133298.
50. **Norman M**, **Ter-Ovanesyan D**, **Trieu W**, **Lazarovits R**, **Kowal EJK**, **Lee JH**, **Chen-Plotkin AS**, **Regev A**, **Church GM**, **Walt DR.** L1CAM is not associated with extracellular vesicles in human cerebrospinal fluid or plasma. *Nat Methods* 18: 631–634, 2021. doi:10.1038/s41592-021-01174-8.
51. **Gomes DE**, **Witwer KW.** L1CAM-associated extracellular vesicles: A systematic review of nomenclature, sources, separation, and characterization. *J Extracell Biol* 1: e35, 2022. doi:10.1002/jex2.35.
52. **Baeyens L**, **Hindi S**, **Sorenson RL**, **German MS.** β-Cell adaptation in pregnancy. *Diabetes Obes Metab* 18: 63–70, 2016. doi:10.1111/dom.12716.
53. **Freemark M**, **Avril I**, **Fleenor D**, **Driscoll P**, **Petro A**, **Opara E**, **Kendall W**, **Oden J**, **Bridges S**, **Binart N**, **Breant B**, **Kelly PA.** Targeted deletion of the PRL receptor: effects on islet development, insulin production, and glucose tolerance. *Endocrinology* 143: 1378–1385, 2002. doi:10.1210/endo.143.4.8722.
54. **Huang C**, **Snider F**, **Cross JC.** Prolactin receptor is required for normal glucose homeostasis and modulation of beta-cell mass during pregnancy. *Endocrinology* 150: 1618–1626, 2009. doi:10.1210/en.2008-1003.
55. **Nteeba J**, **Kubota K**, **Wang W**, **Zhu H**, **Vivian JL**, **Dai G**, **Soares MJ.** Pancreatic prolactin receptor signaling regulates maternal glucose homeostasis. *J Endocrinol* 241: 71–83, 2019. doi:10.1530/JOE-18-0518.
56. **Shrivastava V**, **Lee M**, **Lee D**, **Pretorius M**, **Radford B**, **Makkar G**, **Huang C.** Beta cell adaptation to pregnancy requires prolactin action on both beta and non-beta cells. *Sci Rep* 11: 10372, 2021. doi:10.1038/s41598-021-89745-9.
57. **Sorenson RL**, **Brelje TC.** Prolactin receptors are critical to the adaptation of islets to pregnancy. *Endocrinology* 150: 1566–1569, 2009. doi:10.1210/en.2008-1710.
58. **Ilekis JV**, **Tsilou E**, **Fisher S**, **Abrahams VM**, **Soares MJ**, **Cross JC**, **Zamudio S**, **Illsley NP**, **Myatt L**, **Colvis C**, **Costantine MM**, **Haas DM**, **Sadovsky Y**, **Weiner C**, **Rytting E**, **Bidwell G.** Placental origins of adverse pregnancy outcomes: potential molecular targets- an executive workshop summary of the Eunice Kennedy Shriver National Institute of Child Health and Human Development. *Am J Obstet Gynecol* 215: S1–S46, 2016. doi:10.1016/j.ajog.2016.03.001.
59. **Lee E**, **Kazemi P**, **Shafiei S**, **Yull S**, **Rana M**, **Tawil N**, **Montermini L**, **Rak J**, **Dufort D.** Extracellular vesicles as prospective biological indicators for midgestational placental complications in the mouse. *Front Cell Dev Biol* 13: 1636335, 2025. doi:10.3389/fcell.2025.1636335.
60. **Ortega MA**, **Fraile-Martínez O**, **García-Montero C**, **Paradela A**, **Asunción Sánchez-Gil M**, **Rodriguez-Martin S**, **De León-Luis JA**, **Pereda-Cerquella C**, **Bujan J**, **Guijarro LG**, **Alvarez-Mon M**, **García-Honduvilla N.** Unfolding the role of placental-derived extracellular vesicles in pregnancy: from homeostasis to pathophysiology. *Front Cell Dev Biol* 10: 1060850, 2022. doi:10.3389/fcell.2022.1060850.
61. **Forhead AJ**, **Fowden AL.** The hungry fetus? Role of leptin as a nutritional signal before birth. *J Physiol* 587: 1145–1152, 2009. doi:10.1113/jphysiol.2008.167072.
62. **Henson MC**, **Castracane VD.** Leptin in pregnancy. *Biol Reprod* 63: 1219–1228, 2000. doi:10.1095/biolreprod63.5.1219.
63. **Pérez-Pérez A**, **Toro A**, **Vilariño-García T**, **Maymó J**, **Guadix P**, **Dueñas JL**, **Fernández-Sánchez M**, **Varone C**, **Sánchez-Margalet V.** Leptin action in normal and pathological pregnancies. *J Cell Mol Med* 22: 716–727, 2018. doi:10.1111/jcmm.13369.
64. **Smith TI**, **Russell AE.** Extracellular vesicles in reproduction and pregnancy. *Extracell Vesicles Circ Nucl Acids* 3: 292–317, 2022. doi:10.20517/evcna.2022.27.
65. **Salomon C**, **Scholz-Romero K**, **Sarker S**, **Sweeney E**, **Kobayashi M**, **Correa P**, **Longo S**, **Duncombe G**, **Mitchell MD**, **Rice GE**, **Illanes SE.** Gestational diabetes mellitus is associated with changes in the

concentration and bioactivity of placenta-derived exosomes in maternal circulation across gestation. *Diabetes* 65: 598–609, 2016. doi:10.2337/db15-0966.

66. **Taylor J**, **Jaiswal R**, **Bebawy M.** Calcium-calpain dependent pathways regulate vesiculation in malignant breast cells. *Curr Cancer Drug Targets* 17: 486–494, 2017. doi:10.2174/1568009616666161026165736.
67. **Taylor J**, **Azimi I**, **Monteith G**, **Bebawy M.** Ca^{2+} mediates extracellular vesicle biogenesis through alternate pathways in malignancy. *J Extracell Vesicles* 9: 1734326, 2020. doi:10.1080/20013078.2020.1734326.
68. **Liu YJ**, **Wang C.** A review of the regulatory mechanisms of extracellular vesicles-mediated intercellular communication. *Cell Commun Signal* 21: 77, 2023. doi:10.1186/s12964-023-01103-6.
69. **Stahl PD**, **Raposo G.** Extracellular vesicles: exosomes and microvesicles, integrators of homeostasis. *Physiology (Bethesda)* 34: 169–177, 2019. doi:10.1152/physiol.00045.2018.
70. **Yu D**, **Mei Y**, **Wang L**, **Zhao Y**, **Fan X**, **Liang D**, **Li L**, **Zhu J**, **Bi S**, **Wang X**, **Qi Z**, **Zhu L**, **Wang Y.** Nano-seq analysis reveals different functional tendency between exosomes and microvesicles derived from hUMSC. *Stem Cell Res Ther* 14: 272, 2023. doi:10.1186/s13287-023-03491-5.
71. **Kampmann U**, **Knorr S**, **Fuglsang J**, **Ovesen P.** Determinants of maternal insulin resistance during pregnancy: an updated overview. *J Diabetes Res* 2019: 5320156, 2019. doi:10.1155/2019/5320156.
72. **Sonagra AD**, **Biradar SM**, **K D**, **Murthy DSJ.** Normal pregnancy- a state of insulin resistance. *J Clin Diagn Res* 8: CC01–CC03, 2014. doi:10.7860/JCDR/2014/10068.5081.
73. **Rassie K**, **Giri R**, **Joham AE**, **Teede H**, **Mousa A.** Human placental lactogen in relation to maternal metabolic health and fetal outcomes: a systematic review and meta-analysis. *Int J Mol Sci* 23: 15621, 2022. doi:10.3390/ijms232415621.
74. **Barbour LA**, **Shao J**, **Qiao L**, **Pulawa LK**, **Jensen DR**, **Bartke A**, **Garrity M**, **Draznin B**, **Friedman JE.** Human placental growth hormone causes severe insulin resistance in transgenic mice. *Am J Obstet Gynecol* 186: 512–517, 2002. doi:10.1067/mob.2002.121256.